Ionospheric Scintillation Monitoring Using Commercial Single Frequency C/A Code Receivers*

A. J. Van Dierendonck
AJ Systems

John   Klobuchar
US *Air Force Phillips Laboratory*

Quyen Hua
PAQ Communications

BIOGRAPHIES

Dr. A. J. Van Dierendonck received his BSEE from South Dakota State University and MSEE and PhD from Iowa State University. Currently, he is on temporary assignment as Principal SatNav Advisor with Inmarsat, London. Previously self-employed, as AJ Systems, he provided GPS expertise to numerous companies, including PAQ Communications, NovAtel and Inmarsat. A. J. has 20 years of GPS experience.

John Klobuchar is a senior Physical Scientist in the Ionospheric Effects Division of the Air Force Phillips Laboratory. He is an international expert on ionospheric electron content, and ionospheric effects on Air Force Systems. He is a Fellow of the IEEE and a consultant to numerous Air Force and DOD programs.

Dr. Quyen Hua received his BSEE, MSEE, MBA and PhD from Ohio University. He has 16 years of experience in GPS systems and software engineering. He is currentlv a self-employed under the name of PAQ Communications.

ABSTRACT

The earth's ionosphere can cause serious problems for many radio applications: DOD C^3I and navigation systems and commercial applications such as communications, radio astronomy and navigation. They can all be seriously affected by ionospheric disturbances. Disturbance effects such as amplitude fading and phase scintillation limit the ability to coherently integrate weak signals. One solution, which reduces the effective data capacity of the channel, is the use of time-interleaved modulation schemes in which data is sent repeatedly to ensure its error-free reception. Another solution is to use alternate resources during the times of predicted signal outages due to scintillation fading. However, these predictions are generally based on monthly climatology and are poor for a specific time in a particular region due to the variability and dynamics of the earth's ionosphere. A more real-time and local solution is required

GPS signals provide an excellent means for measuring scintillation effects on a disperse global basis because they are continuously available and can be measured through many points of the ionosphere simultaneously. GPS signals are themselves affected, but because of the spread spectrum properties of the signal, tracking through disturbances with a GPS receiver is usually possible with reasonably wide bandwidth tracking loops. and scintillation parameters can be extracted There are GPS applications, however, such as surveying where integrated carrier phase measurements are used, in which scintillation can easily disrupt operational activities [l].

This paper presents the result of a Small Business Innovative Research (SBIR) Phase I study and testing of a software-modified commercial C/A code receiver to perform this function. The result is a design of a low-cost, portable Ionospheric Scintillation Monitor (ISM) being developed on a follow-on SBIR Phase II project.

INTRODUCTION

In the past_ the monitoring of ionospheric scintillation using satellite radiated signals has primarily been on an experimental basis. Specially designed satellites have been launched for that purpose [2]   In more recent years, the signals radiated from the GPS satellites have been used with success, but mostly experimental [3. 4]. Although GPS signals provide an excellent means of operationally monitoring ionospheric scintillation, it has

been done on a limited scale. This is because off-the-shelf GPS receivers do not provide the phase and amplitude information required for scintillation parameter extraction. Specially modified receivers have to be used.

In the past, dual frequency P code receivers have been used (experimentally) measuring differenced L1/L2 phase measurements. This differencing cancels all other systematic effects such as satellite motion, clocks, selective availability and the troposphere. Unfortunately, the cost of these receivers and the looming threat of Anti-Spoof (A-S) encryption of the P code has prevented this exploitation on an operational basis. Codeless cross-correlation receivers that will operate with A-S encryption present are available, but their measurements are either far too noisy or are too bandwidth limited to be of use for ionospheric scintillation monitoring

In the studies and testing reported here. the systematic effects are removed by high-pass filtering Ll only measurements rather than differencing Ll and L2 phase measurements. This solution takes advantage of the latest commercial GPS receiver technology and provides a local monitoring system that is practical for low-cost deployment in large numbers in a theater battlefield environment, as well as for commercial satellite communications.

The use of a low-cost commercial GPS receiver is key to this program. Not only is the cost of such a receiver much less than that of military type receivers, but crypto-keys are not required for its operation. Even if one were to use a commercial dual frequency P code receiver with code encryption capabilities added, the logistic costs and procedures for using crypto-keys would impair the usefulness in large numbers and in remote areas. Of course, the requirement for these keys would make it virtually impossible for use in commercial applications. Since codeless cross-correlation receivers that overcome the P code encryption are too noisy, we are left with no alternative but to use the single Ll frequency modulated with CIA code.

The key to using a single frequency is the ability to remove the low frequency systematic effects. Upon undertaking this study, it was suspected that_ for an off-the-shelf commercial receiver, the receiver oscillator's phase noise could not be removed by filtering, and by far would dominate what would be expected of phase scintillation variations. All other systematic effects should easily be removed, including Selective Availability (SA). Mostly, this was found to be true, although more testing is needed to verify that SA is totally removed. Fortunately, by replacing the standard temperature compensated crystal oscillator (TCXO) with a high quality oven-

controlled crystal oscillator (OCXO). this dominant effect is reduced to desired levels.

The ability to extract amplitude scintillation parameters was also studied and tested. The use of a single frequency does not impair the ability to do this at all. This is how it is usually done. In fact, since the GPS C/A code signal is 3 dB stronger than the P code signal, its use provides an advantage, although multipath fading effects could be more significant. However, the receiver chosen for this testing, the NovAtel Model 951 GPSCard™, is known for is multipath mitigation capability [5].

The Phase II effort of this program has just begun. During the Phase I effort, data was collected and the scintillation analysis was performed off-line. During the Phase II effort, an inexpensive portable C^3I Ionospheric Scintillation Monitor (ISM) will be developed to measure and provide, in real-time, parameters of the ionospheric scintillation environment.

PHASE I ANALYSIS

The systems engineering activity performed during the Phase I activities includes the following:

> 1) The derivation of the algorithms used in determining phase and amplitude scintillation parameters for the ISM
>
> 2) Analysis of predicted performance of the ISM,
>
> 3) Results of testing the algorithms and performance of the ISM.

The key results of the analysis and testing are the following:

> 1) A high performance low-phase noise reference oscillator is required when using a single frequency GPS receiver to monitor ionospheric phase scintillation,
>
> 2) Care must be taken to insure minimal signal multipath for the determination of low level amplitude scintillation.
>
> 3) The feasibility of using a modified low-cost, but high performance, commercial GPS receivers for ionospheric scintillation monitoring is proven.

First phase scintillation measurement algorithms and performance are discussed. Then, amplitude scintillation measurement algorithms and performance are discussed.

Phase Scintillation

Phase **scintillation monitoring is** traditionally accomplished by monitoring the standard deviation, $\sigma_{\Delta\phi}$, and the power spectrum of detrended carrier phase from signals received from satellites, which in this case are GPS satellites. In the Phase I effort, determination of power spectrum parameters, namely the spectral slope (p) and spectral strength (T), was not performed. However, the capability of recording raw detrended phase data for off-line spectral analysis is provided. The $\sigma_{\Delta\phi}$'s are computed (off-line), however, over 1, 3, 10, 30 and 60 second intervals every 60 seconds. The 1, **3, 10 and 30** second interval $\sigma_{\Delta\phi}$'s are then averaged over the 60 second interval. These five values are stored on a tile and displayed for each satellite along with a time tag, the satellite PRN number and azimuth and elevation angles and the latitude, longitude and altitude location of the monitoring site. These later values are intended to determine, off-line, the Ionospheric Penetration Point (IPP) The option to record raw detrended phase data, at a 50 Hz rate. can be selected by the operator. The raw phase data has a noise bandwidth of 15 Hz. Raw phase data (not detrended) are always recorded, but only on a temporary **basis. The data** is overwritten during subsequent collection periods.

In this section, the algorithms for phase detrending are described. Since the receiver used on the Phase I effort of this program, the NovAtel Model 951 **GPSCard™**, uses a small low-powered TCXO as its timing reference, the possibility of phase scintillation monitoring contamination existed. Thus, testing and analysis was performed to determine the effects of oscillators. It was found that the TCXO phase noise obscures the effects of low level phase scintillation. Through testing with an Oven Controlled Crystal Oscillator (OCXO), it was found that the OCXO phase noise does not obscure the effects of low level phase scintillation.

Phase Detrending Algorithms

In the use of GPS in the past for experimental scintillation sensing, detrended carrier phase data was computed from differenced Ll and L2 measurements. Then, the effects of integrated doppler due to satellite motion, satellite clocks (including SA), user clocks and the tropospheric delay cancel in the differencing. Ll only carrier phase data includes all these effects. In case of the differenced Ll and L2 measurements, the only remaining effects are that of the ionosphere itself and unwanted multipath, which is limited to less than one fourth of a carrier cycle. This *is* also the goal for detrended Ll measurements.

The method used for detrending passes the phase measurements through a high-pass filter, which removes all low frequency effects below its frequency cut-off. This method has been used in the past by ionospheric scintillation researchers [2]. The GPS satellite doppler dynamics are much less than the satellite observed in that study, suggesting that this type of detrending should work even better using GPS. A question remains, however, whether or not SA and the user's clock effects could be removed successfully.

Digital High-Pass Filter Implementation. A sixth-order Butterworth filter with a 0.1 Hz 3dB cutoff frequency was used to filter out the low frequency data_ similar to that used in *[2]*. There, the input data was sampled at 100 samples-per-second (sps), but sampling at 50 sps is sufficient for the 15 Hz noise bandwidth. The filter has a form in the s-plane as shown in Figure 1, where [6]

$$Y_i(s) = \frac{s^2}{s^2 + a_i \omega_N s + \omega_N^2} \qquad 1)$$

where

$$f_N = \frac{\omega_N}{2\pi} \qquad 2)$$

is the filter's comer frequency in Hz. The coeffkients take on the values

$$a_1 = \sqrt{2 + \sqrt{3}} = 1931851652578 \qquad 3)$$

$$a_2 = \sqrt{2} = 1.414213562 \qquad 4)$$

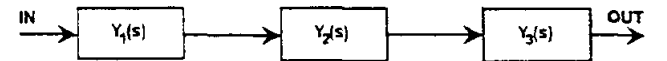$$a_3 = \sqrt{2 - \sqrt{3}} = 0.517638090205 \qquad j)$$

Figure 1. Sixth-Order Butterworth **Filter**

The product $Y_1(s)Y_2(s)Y_3(s)$ makes up the **LaPlace** Transform of a high-pass filter with a frequency response of

$$|Y(jf)|^2 = \frac{f^{12}}{f^{12} + f_N^{12}} \qquad 6)$$

This filter is implemented in the time domain using the equations presented in Appendix I.

Using Detrending Phase Algorithms with Measured Data Raw integrated phase data was collected from seven satellites on 3 November 1992. The purpose of this collection was to test the detrending algorithms as well as to determine the effects of the TCXO phase noise on the detrended data.

Figure 2 shows a plot of the detrended phase residuals using a 0.1 Hz filter cutoff *frequency* for two different satellites (PRNs 18 and 16), each having a different received C/N_o. The time scale is arbitrary since the data from the two satellites were not collected at the same time. The standard deviation of the phase over the period of the plots is also indicated, which are on the order of that experienced at L-band during active scintillation periods reported in [2]. Obviously. this is not acceptable as scintillation could not be monitored. The predominate phase noise is due to the TCXO flicker noise. To verify this, the simultaneous accumulated phases between two different satellites were differenced and detrended, which eliminated the common effects of the TCXO. This detrended phase is plotted in Figure 3 for PRNs 18 and 27. Note that the noise is now nearly white and at a much lower level, even though it is the sum of the noises of two independent signals.   There still appears to be some lower *frequency* component, which could be a combination of multipath, the satellites' frequency references or SA, which do not cancel. The standard deviation is only 0.0775 radians, a quite acceptable level, which also verities that the detrending does remove all systematic effects, at least over the periods observed. Although this differencing provides excellent results, the method is not as desirable in determining scintillation characteristics from individual satellites, since the IPP of the disturbance is not readily determined. However. by differencing between a number of satellites, the IPPs could be inferred through a process of elimination. This *is* a point to be considered in the future for the purpose of reducing hardware costs.
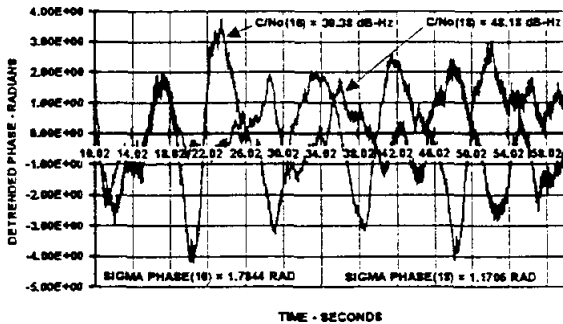

Figure 2. Detrended Phase Noise with a **Filter Cutoff Frequency of 0.1 Hz for Two Satellites**
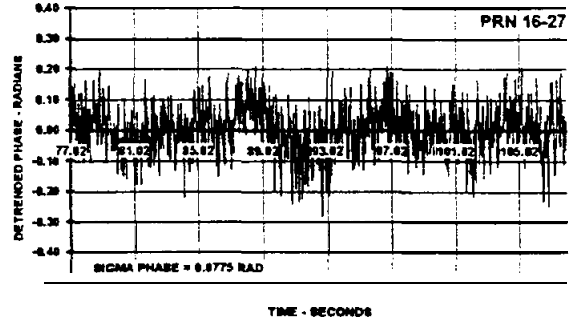

Figure 3. Detrended Differential Phase Between Two Satellites

Oscillator Phase Noise Evaluation It was obvious that something had to be done to eliminate this TCXO flicker noise. One solution is to use a better oscillator. However. TCXOs with better phase noise characteristics are not available. especially those of the size present on the NovAtel GPSCard™. OCXOs do have better phase noise characteristics. One such oscillator was analyzed to verify that its performance would be acceptable to this application. This oscillator is a Vectron OCXO specially designed for operation with the GPSCard™, although it operates external to the GPSCard™.

Predicted Oscillator Performance. Figure 4 presents the predicted high-pass filtered phase noise spectral density of both the TCXO and the OCXO at the GPS Ll frequency. Also shown are the high-passed phase noise densities due to thermal noise at C/N_os of 30 and 50 dB-Hz and high-passed SA. Note that the phase noise density of the TCXO far exceeds that of thermal noise, while the phase noise density of the OCXO is comparable. Furthermore, the phase noise density of the OCXO is generally two orders of magnitude lower than that of the TCXO. These spectral densities were derived from the respective oscillator specifications.
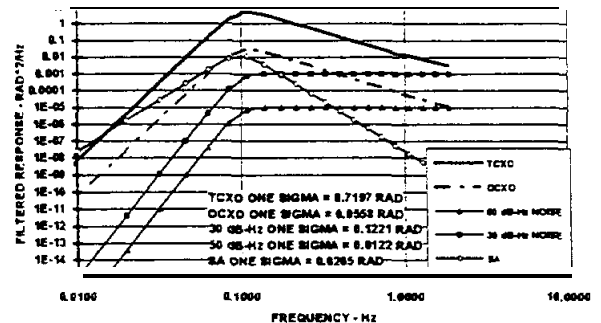

Figure 4. Predicted Spectral Density of Dctrended Oscillator, Ambient Phase Noise and SA

The standard deviations of the phase for the spectral densities of Figure **4** were determined by integrating over

4

the interval shown extended to the receiver's tracking loop noise bandwidth of 15 Hz. The resulting one sigma phase noise values are shown on the graph. Note that the TCXO and thermal noise values am compatible with that obtain in the analysis described above in Figures 2 and 3. Also note that the OCXO value is quite acceptable for monitoring phase scintillation at L-band [2].

Measured OCXO Performonce. Phase data using the OCXO was collected and analyzed. The results are presented here. Figure 5 shows detrended phase using the OCXO for data collected from PRN 11 on 24 November 1992 as compared to **the data using the** TCXO presented above for PRN 16. Note that the high level phase noise evident with the TCXO is no longer present,   There is still some low level low frequency oscillations It is suspected that these oscillations are due to a combination of multipath and the OCXO. Since SA is not present on PRN 11, it is not due to SA. Some of the oscillations correlate with suspected multipath presented later. The RMS phase errors are indeed at least an order of magnitude less than those using the TCXO, which was predicted. They are also at acceptable levels for phase scintillation measurements.

Summarv Detrended **Phase Results** The 1, 3, 10, 30 and 60 second interval $\sigma_{\Delta\phi}$'s over a 27 minute collection period for satellite PRN 11 are plotted in Figure 6 and compared to the theoretical $\sigma_{\Delta\phi}$ This value is the root-sum-squared of the predicted phase error due to the OCXO phase noise and thermal noise, which. for that collection period, is mostly the OCXO phase noise. The l-second $\sigma_{\Delta\phi}$'s are generally less than the theoretical value. This is because the OCXO phase noise is dominated by lower frequency noise -- probably flicker noise. Also, the IO-second $\sigma_{\Delta\phi}$'s are lower in value than the 3-second $\sigma_{\Delta\phi}$'s, indicating that the flicker noise is partially eliminated in the linear detrending process. The 30 and 60-second $\sigma_{\Delta\phi}$'s are nearly the same that is probably due to multipath.
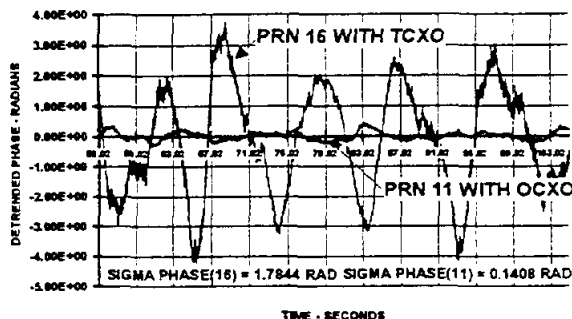

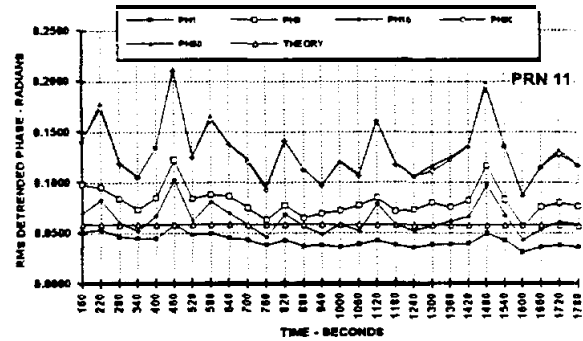**Figure 5. Detrcnded Phase Noise Comparing** TCXO and OCXO **Performance**

Figure 6. Summary of Detrended Phase Standard Deviations using an OCXO

The **Effects of** SA Unfortunately, as indicated above. the only data analyzed during the Phase I program when using the good oscillator, happened to not include the effects of SA. These effects will be studied further during the Phase JI activities. However, using spectral analysis based upon spectral characteristics of SA measured by others [7], the effects of SA on the measurement of phase scintillation can be predicted. The results of this spectral analysis are shown in Figure 4. Those results indicate that the effects of SA are less than, but close to. those of the OCXO. Also, the two satellites differenced in Figure 3 both had SA on. The phase noise plotted in that figure would verify the analysis prediction. However, that is too little data tc come to a sound conclusion. More testing has to be performed for that.

Amplitude Scintillation

Amplitude scintillation monitoring is traditionally accomplished by monitoring the index S4. The S4 index is derived from detrended signal intensity of signals received from satellites. Signal intensity is actually received signal power, which is measured in a way that its value doesn't fluctuate with noise power. Thus, it can't be based upon signal-to-noise density or ratio. Also. it is imperative that the receiver's noise Automatic Gain Control (AGC) be disabled when these measurements are taken so that the AGC doesn't alter the measured signal intensity. Since the S4 index is normalized, the receiver's absolute gain is not important, as long as it is relatively constant during the deuending period. It is also important that the intensity measurement be linear with respect to the signal power over its entire range. including deep scintillation fades.

S4 measured at L-band needs to have the effects due to ambient noise removed, since the ambient noise at the Ll frequency translates to a relatively high S4 at lower frequency VHF and UHP frequencies.   It is desired that the

resulting S4 **value** be **less** than **0. 05** for all **received signal levels above -139 dBm**.

The S4 values are normally computed over 60 second intervals. In the ISM, values are stored on a file and displayed for each satellite along with the storage and display of the phase data as described earlier. As noted below, the standard deviation of the code/carrier divergence is also computed over the same 60 second interval and stored as an indicator of multipath activity. The recording of raw detrended intensity data, at a 50 Hz rate, can be selected by the operator. The raw intensity data has a single-sided noise bandwidth of 25 Hz.

The S4 Measurement The raw intensity measurement having the characteristics stated above is the difference between Narrow Band and Wide Band Power (NBP and WBP), measured over the same interval every 20 milliseconds, where

$$WBP = \sum_{i=1}^{20} I_i^2 + Q_i^2 \qquad 7)$$

and

$$NBP = \left(\sum_{i=1}^{20} I_i\right)^2 + \left(\sum_{i=1}^{20} Q_i\right)^2 \qquad 8)$$

where I, and Q_i are the 1 kHz in-phase and quadraphase samples. If the receiver's gain is constant this difference is proportional to received signal power S, or signal intensity SI. Then, the total S4. including the effects of ambient noise, is defined as follows:

$$S4_T = \sqrt{\frac{\langle SI^2 \rangle - \langle SI \rangle^2}{\langle SI \rangle^2}} \qquad 9)$$

where (.) represents the expected (or average) value over the interval of interest (60 seconds).

S4 Detrending As with the phase measurements, the intensity measurements must be detrended. The received signal power varies due to changing range, antenna patterns and multipath. According to [2], this can be done by filtering the intensity measurements in a low-pass filter that is similar to the high-pass filter described above and Appendix I. The differences are as follows:

1) The transfer function of each filter stage is of the form

$$Y_i(s) = \frac{\omega_N^2}{s^2 + a_i \omega_N s + \omega_N^2} \qquad 10)$$

resulting in an overall frequency response of

$$|Y(jf)|^2 = \frac{f_N^{12}}{f^{12} + f_N^{12}} \qquad 11)$$

2) The detrending is accomplished by dividing the input by the output of the low-pass filter as

$$SI_k = \frac{(NBP - WBP)_k}{(NBP - WBP)_{lpf,k}} \qquad 12)$$

which fluctuates around a value of 1.

3) The cutoff frequency is not necessarily the same as for phase detrending. The capability of entering a different value for f_N for intensity detrending is included.

4) The low-pass filter used for detrending has different time-domain equations than the high-pass filter, and are provided in Appendix I.

Removing, the Effects of Ambient Noise Unfortunately, the total S4 defined in Equation 9 can have significant values simply due to ambient noise. Since this index would be used in practice by scaling to predict amplitude scintillation at lower frequencies, such as VHF and UHF any value due to noise at Ll can swamp out low amplitude scintillation that scale to significant levels at VI-IF and UHF. Thus, it is desirable to remove, as well as one can, the effects of ambient noise. This can be done by estimating the average signal-to-noise density over the entire evaluation interval (60 seconds), and using that estimate to determine the expected S4 due to ambient noise. This is legitimate since the amplitude scintillation fades do not significantly alter the average signal-to-noise density over a 60 second time interval

Note from Equation 9 that S4 is simply the square-root of the normalized variance of signal power. If the signal-to-noise density (S/N_o) is known, the predicted S4 due to ambient noise is

$$S4_{N_o} = \sqrt{\frac{100}{S/N_o}\left[1 + \frac{500}{19\,S/N_o}\right]} \qquad 13)$$

Thus, by replacing the S/N_o with the 60 second estimate **i/if., an** estimate of signal-to-noise density, we obtain an estimate of the S4 due to noise $S4_{N_o}$ Subtracting the square of this value from the square of Equation 9 yields the revised value of S4

$$S4 = \sqrt{\frac{\langle SI^2 \rangle - \langle SI \rangle^2}{\langle SI \rangle^2} - \frac{100}{\hat{S}/\hat{N}_o}\left[1 + \frac{500}{19\hat{S}/\hat{N}_o}\right]} \quad 14)$$

When there is no scintillation the value under the radical may go slightly negative. If it does, we are truly removing the effects of ambient noise. This problem can be eliminated by simply setting S4 to zero in those cases.

Testing S4 with Measurement Data and the Effects of Multipath. The same data used to test the phase detrending and statistics were also used to test the S4 algorithms. S4 was computed each 60 seconds of a thirty-three minute data collection period from satellite PRN 11 on 24 November 1992. The summary results are shown in Figure 7. Note that tbe S4 started high and then diminished with time. during which time the elevation angle to the satellite became larger. Note also the difference between the uncorrected S4 computed using Equation 9 and the corrected value using Equation 14. It appears that this correction does not remove the effects of rapidly varying multipath.
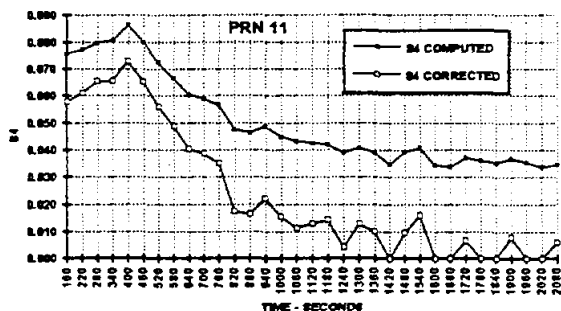

Figure 7. Thirty-Three Minutes of S4

The Effects of Multipath on S4. Multipath affects S4 because it causes fading of the received signal due to cross-correlation with the multipath signal. Also, delay-lock-loop tracking errors tend to "pull" the carrier tracking point away from the true correlation peak, also causing a reduction in signal correlation amplitude. Long term effects of multipath are removed with detrending. However, multipath from closer-in objects will give short term effects that are observed here.

The larger values of S4 early in the collection period are due to multipath, even though the GPSCard™ receiver and GPSAntenna™ antenna have natural multipath rejection capabilities [5]. Thus, care must be taken to ensure a multipath-free environment, *or the* use of multipath mitigation instruments such as antenna choke rings. No such care was taken in the collection of the subject data. The antenna was placed on a roof with many multipath sources.

Variations in the code/wrier divergence. which is the measured difference between group delay and carrier phase advance, can be used to verify the existence of multipath. This is because the group delay tracking ERROR due to multipath far exceeds carrier tracking errors due to multipath. There is also a divergence due to the ionosphere, but one would not expect this to be significant over a 60 second period. Thus, the standard deviation of the code/carrier divergence can be used as a measure of multipath presence, given as

$$\sigma_m = \sqrt{\sigma_{div}^2 - \sigma_N^2}$$
$$= \sqrt{\sigma_{div}^2 - \frac{1}{1540^2}\frac{B_L d}{2\hat{S}/\hat{N}_o}\left(1 + \frac{100}{\hat{S}/\hat{N}_o}\right)} \quad 15)$$

where B_L is the code tracking loop noise bandwidth. d is the correlator spacing and $\hat{S}/\hat{N}_o$ is the same estimated signal-to-noise density used in Equations 13 and 14 above. B_L and d are 0.05 Hz and 0.1 chips, respectively, for the Model 951 GPSCard™. The second term under the radical removes the estimated variations due to ambient noise [5]. The mean divergence and these standard deviations are indicated in Figure 8 for the thirty-three minute collection period.
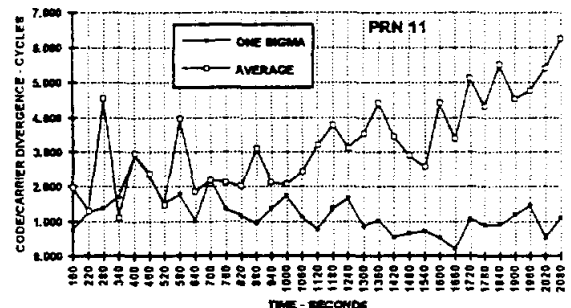

Figure 8. Thirty-Three Minutes of Divergence

The standard deviation σ_m of Equation 15 is computed over every 60-second interval and stored along with the associated S4 value. Although the σ_m's are not foolproof indications, they do provide some indication of multipath. For example, if the value is *greater than. say,* 1.5 cycles, the S4 is generally greater than 0.05.

Detrended Intensity From Satellite PRN Il. Figures 9, 10 and 11 **provide** snapshots of detrended intensity and divergence over this thirty-three minute period of collection. Changes in intensity are certainly correlated to rapid changes in the divergence. In Figure 9 (Run 5), the intensity fluctuates about 0.5 dB. The S4 is relative high and so is the standard deviation of the divergence (Figure 11). In Figure 10 (Run 7), the intensity is rather quiet. The S4 is very low and the standard deviation of the

divergence is also relatively low. Figure 11 shows a significant change **in the code/carrier divergence between those two l-minute periods.** The variations correlate well with the larger values of S4.
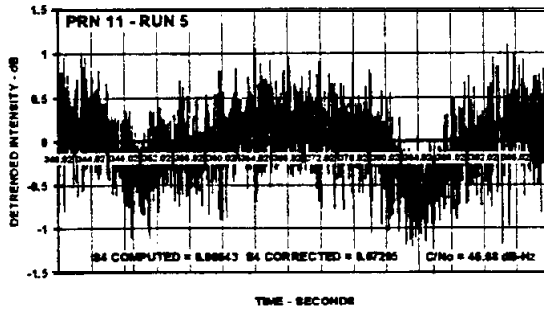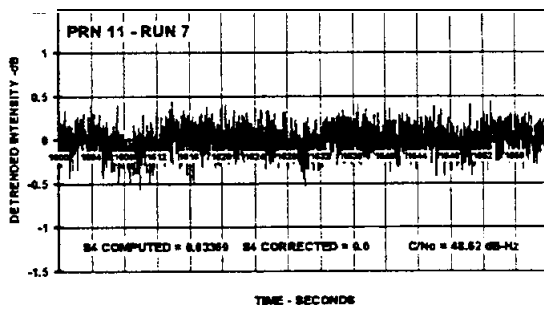

Figure 9. Detrended Intensity - 340 to 400 Seconds

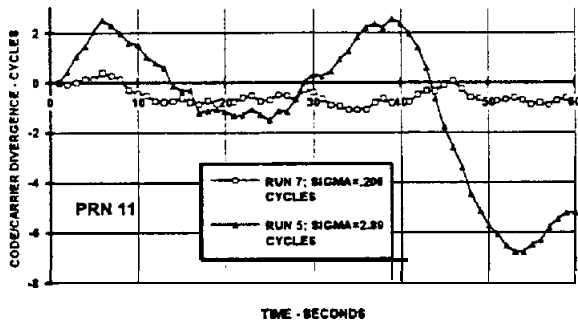**Figure 10. Detrended Intensity - 1600 to 1660 Seconds**

Figure 11. Code/Carrier Divergence - Runs 5 and 7

PHASE II ENHANCEMENTS

The objective of the Phase II SBIR effort is to complete the development of the ISM and deliver units to the U. S. Air Force for testing in a disturbed ionospheric environment. The Phase II units will be portable, operate unattended and output scintillation parameters in real-time, requiring both software and hardware enhancements.

Software Enhancements

During the Phase II effort, the software of the ISM will be upgraded so that the detrending and the computation of the RMS residuals and spectral parameters will be per-

formed in real-time for signals from up to 10 GPS satellites simultaneously. RMS residuals will be computed and stored and displayed every 60 seconds.

Phase Spectral Parameters The spectral parameters are strength T and slope p defined such that the phase spectrum

$$\Phi_\phi(v) = Tv^{-p} \qquad\qquad 16)$$

is a fit to a computed frequency line spectrum. This fitting is done over the frequency range 0.5 Hz < v < 10 Hz. The line spectrum will be computed using a 4,096-point Fast Fourier Transform (FFT) on 81.92 seconds of 50 Hz phase data every 60 seconds. Every 60 seconds, a new set of 3.000 points is combined with the last 1,096 points of the previous 60 **seconds.**

Scaling to Other frequencies The users of the ISM certainly want to know the effect of ionospheric scintillation on the frequency of their application, not the effect on the GPS system at the Ll frequency. The GPS L-band measurements can be scaled to the transmission frequencies of DOD and commercial applications using scaling measures known in the ionospheric scintillation community. The scaling for the amplitude and phase parameters are respectively [2] :

$$S_4(f) = S_4(L1)\left(\frac{f_{L1}}{f}\right)^{1.5} \qquad\qquad 17)$$

$$\sigma_\phi(f) = \sigma_\phi(L1)\frac{f_{L1}}{f} \qquad\qquad 18)$$

Scaling to these various frequencies will be for display purposes only. The users may select up to five frequencies for which the parameters are to be displayed.

Hardware Enhancements

Figure 12 shows the Phase II ISM configuration. The ISM, except for the antenna and optional choke ring and optional DC-AC converter, will fit in a suitcase about the size of a large brief case. The components in the suitcase are a notebook computer, its power supply. a 5- and 12-volt power supply to drive the OCXO and the receiver. a NovAtel OEM GPSCard™, an auxiliary Transputer module and a Eurocard cage.
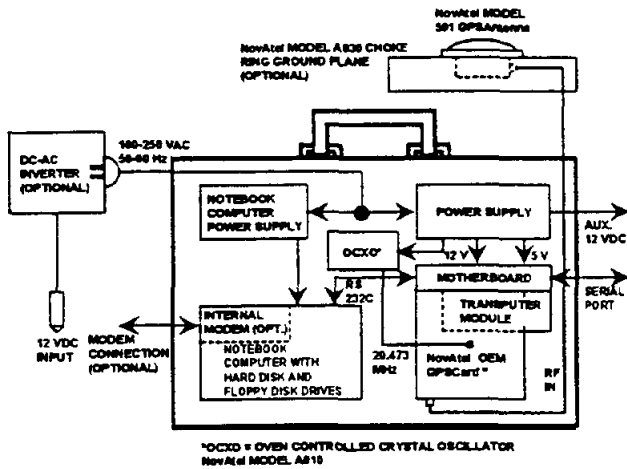
Figure 12. The ISM in a Briefcase

The NovAtel OEM GPSCard™ in a Eurocard format replaces the Model 951 card used in the Phase I testing. A Transputer module that fits in the same Eurocard chassis will be used to provide through-put enhancement to perform the high-speed real-time operations (and FFT). This module contains the identical Transputer embedded on the GPSCard™, to which it will interface via an existing connector.

SUMMARY AND CONCLUSIONS

The feasibility of using a modified high-performance commercial GPS C/A code receiver for ionospheric scintillation parameter estimation has been proven. These modifications include high-speed processing of carrier phase and signal power **measurements to** obtain phase and amplitude scintillation parameters, and the addition of a high quality oven-controlled crystal oscillator (OCXO) as the receiver's frequency reference. Classical ionospheric scintillation parameters were computed from data measured in a non-scintillating environment to show that phase and amplitude measurements provide the quality required to scale these parameters to frequencies of interest.

Plans for the Phase II effort were presented, which includes software enhancements for real-time processing of signals from up to 10 GPS satellites and the development of a low-cost portable Ionospheric Scintillation Measurement (ISM) unit.

APPENDIX L DETRENDING FILTER IMPLEMENTATION

The detrending filters for filtering the systematic effects out of the phase and amplitude measurements are made up of three cascaded second order digital filters satisfying the following equations [8]:

$$\begin{bmatrix} X_{i1} \\ X_{i2} \end{bmatrix}_{k+1} = \begin{bmatrix} \phi_{i11} & \phi_{i12} \\ \phi_{i21} & \phi_{i22} \end{bmatrix} \begin{bmatrix} X_{i1} \\ X_{i2} \end{bmatrix}_k + \begin{bmatrix} \Gamma_{i1} \\ \Gamma_{i2} \end{bmatrix} u_{i,k+1} \quad \text{I.1)}$$

where, for the phase detrending,

$$u_{1,k+1} = \phi_{in,k+1} \quad \text{1.2)}$$

is the $k + 1$ raw phase (accumulated doppler) sample,

$$u_{i,k+1} = u_{i-1,k+1} - X_{i-1,1,k+1}; i = 2,3 \quad \text{1.3)}$$

and

$$\phi_{hpf,k+1} = u_{3,k+1} - X_{31,k+1} \quad \text{I.4)}$$

is the output of the cascaded high-pass filter, where Δt is 20 milliseconds. The state transition matrix and input vector elements are given in Table I.

The detrending of the amplitude measurements is different in the following ways:

1) The input $\phi_{in,k+1}$ of Equation I.2 is replaced with $(NBP - WBP)_{k+1}$.

2) The input to the second and third stages are simply the outputs of the previous stage, where

$$u_{i,k+1} = X_{i-1,1,k+1}; i = 2,3 \quad \text{1.5)}$$

producing an output

$$(NBP - WBP)_{lpf,k+1} = X_{31,k+1} \quad \text{1.6)}$$

3) The input vectors r, are different as indicated in Table I.

ACKNOWLEDGMENT

REFERENCES

1. Lambert Wanninger, "Effects of the Equatorial Ionosphere **on GPS,"** *GPS World, July* 1993, pp. 48 - 54.

Table L State Transition Matrix and Input Vector Elements

$$\phi_{i11} = e^{-a_i \pi f_N \Delta t}\left[\cos\left(\sqrt{4-a_i^2}\,\pi f_N \Delta t\right) - \frac{a_i}{\sqrt{4-a_i^2}}\sin\left(\sqrt{4-a_i^2}\,\pi f_N \Delta t\right)\right]$$

$$\phi_{i12} = \frac{1}{\sqrt{4-a_i^2}\,\pi f_N}\,e^{-a_i \pi f_N \Delta t}\sin\left(\sqrt{4-a_i^2}\,\pi f_N \Delta t\right)$$

$$\phi_{i21} = -\frac{4\pi f_N}{\sqrt{4-a_i^2}}\,e^{-a_i \pi f_N \Delta t}\sin\left(\sqrt{4-a_i^2}\,\pi f_N \Delta t\right)$$

$$\phi_{i22} \approx e^{-a_i \pi f_N \Delta t}\left[\cos\left(\sqrt{4-a_i^2}\,\pi f_N \Delta t\right) + \frac{a_i}{\sqrt{4-a_i^2}}\sin\left(\sqrt{4-a_i^2}\,\pi f_N \Delta t\right)\right]$$

$$\Gamma_{i1} = 1 - e^{-a_i \pi f_N \Delta t}\left[\cos\left(\sqrt{4-a_i^2}\,\pi f_N \Delta t\right) - \frac{a_i}{\sqrt{4-a_i^2}}\sin\left(\sqrt{4-a_i^2}\,\pi f_N \Delta t\right)\right] = 1 - \phi_{i11} \qquad \text{(phase)}$$

$$\Gamma_{i2} = \frac{4\pi f_N}{\sqrt{4-a_i^2}}\,e^{-a_i \pi f_N \Delta t}\sin\left(\sqrt{4-a_i^2}\,\pi f_N \Delta t\right) = -\phi_{i21} \qquad \text{(phase)}$$

$$\Gamma_{i1} = 1 - e^{-a_i \pi f_N \Delta t}\left[\cos\left(\sqrt{4-a_i^2}\,\pi f_N \Delta t\right) + \frac{a_i}{\sqrt{4-a_i^2}}\sin\left(\sqrt{4-a_i^2}\,\pi f_N \Delta t\right)\right] = 1 - \phi_{i22} \qquad \text{(amplitude)}$$

$$\Gamma_{i2} = 2a_i \pi f_N\left[1 - e^{-a_i \pi f_N \Delta t}\cos\left(\sqrt{4-a_i^2}\,\pi f_N \Delta t\right)\right] + \frac{4\pi f_N\left(1-a_i^2/2\right)}{\sqrt{4-a_i^2}}\,e^{-a_i \pi f_N \Delta t}\sin\left(\sqrt{4-a_i^2}\,\pi f_N \Delta t\right) \qquad \text{(amplitude)}$$

$$= a_i \pi f_N\left(2 - \phi_{i11} - \phi_{i22}\right) - \left(1 - a_i^2/2\right)\phi_{i21}$$

2. E. J. Fremouw, R L. Leadabrand, R C. Livingston, M. D. Cousins, C. L. Rino, B. C. Fair and R A. Long, "Early Results from the DNA WideBand Satellite Experiment – Complex-Signal Scintillation," *Radio Science,* Vol. 13, No. 1, January-February 1978, pp. 167 - 187.

3. C. L. Rino, M. D. Cousins and J. A. Klobuchar, "Amplitude and Phase Scintillation Measurements Using the Global Positioning System," *Effects of the Ionosphere on Radiowave Systems,* J. M. Goodman, Editor, U. S. Government Printing Office, Washington, DC, 1981.

4. J. A. Klobuchar, G. J. Bishop and P. H. Doherty, "Total Electron Content and L-Band Amplitude and Phase Scintillation Measurements in the Polar Cap Ionosphere," *AGARD Conference Preprint No. 382, May* 1985, pp. 2.2-1 - 2.2-7.

5. A. J. Van Dierendonck, Pat Fenton and Tom Ford, "Theory and Performance of Narrow Correlator Spacing in a GPS Receiver," *Navigation: The Journal of the Institute of Navigation,* Vol. 39, No. 3, Fall 1992, pp. 265 - 283.

6. James J. Spilker, Jr., *Digital Communications by Satellite* Prentice-Hall, Englewood Hills, New Jersey, 1977.

7. Hsing-Tung Chou, "An Anti-SA Filter for Non-differential GPS Users," *Proceedings of ION GPS-90,* Third International Technical Meeting of the Satellite Division of The Institute of Navigation Colorado Springs, CO, September 19-21,1990, pp. 535 - 542.

8. Robert *Grover* Brown and Patrick Y. C. Hwang, Introduction to Random Signals and Applied Kalman Filtering, Second Edition, John Wiley & Sons, Inc., New York, NY, 1992.